Nuclear resonant scattering experiment with fast time response: Photonuclear excitation of ^{201}Hg

A. Yoshimi,[1,*] H. Hara,[1] T. Hiraki,[1] Y. Kasamatsu,[2] S. Kitao,[3] Y. Kobayashi,[3] K. Konashi,[4] R. Masuda,[3] T. Masuda,[1] Y. Miyamoto,[1] K. Okai,[5] S. Okubo,[5] R. Ozaki,[5] N. Sasao,[1] O. Sato,[5] M. Seto,[3] T. Schumm,[6] Y. Shigekawa,[2] S. Stellmer,[6] K. Suzuki,[5] S. Uetake,[1] M. Watanabe,[4] A. Yamaguchi,[7] Y. Yasuda,[2] Y. Yoda,[8] K. Yoshimura,[1] and M. Yoshimura[1]

[1]*Research Institute for Interdisciplinary Science, Okayama University, 3-1-1 Tsushima-naka, Kita-ku, Okayama 700-8530, Japan*

[2]*Department of Chemistry, Graduate School of Science, Osaka University 1-1 Machikaneyama Toyonaka, Osaka 560-0043, Japan*

[3]*Research Reactor Institute, Kyoto University, Kumatori-cho, Sennan-gun, Osaka 590-0494, Japan*

[4]*International Research Center for Nuclear Materials Science, Institute for Materials Research, Tohoku University, 2145-2, Narita-cho, Oarai-machi, Higashiibaraki-gun, Ibaraki 311-1313, Japan*

[5]*Graduate School of Natural Science and Technology, Okayama University, 3-1-1 Tsushima-naka, Kita-ku, Okayama 700-8530, Japan*

[6]*Institute for Atomic and Subatomic Physics, TU Wien, 1020 Vienna, Austria*

[7]*RIKEN, 2-1 Hirosawa, Wako, Saitama 351-0198, Japan*

[8]*Japan Synchrotron Radiation Research Institute, 1-1-1 Kouto, Sayo-cho, Sayo-gun, Hyogo 679-5198, Japan*

(Received 17 May 2017; revised manuscript received 21 December 2017; published 8 February 2018)

Nuclear resonant excitation and detection of its decay signal for the 26.27-keV level of ^{201}Hg is demonstrated with high-brilliance synchrotron radiation (SR) and a fast x-ray detector system. This SR-based photonuclear excitation scheme, known as nuclear resonant scattering (NRS) in the field of materials science, is also useful for investigating nuclear properties, such as the half-lives and radiative widths of excited nuclear levels. To date, because of the limited time response of the x-ray detector, the nuclear levels to which this method could be applied have been limited to the one whose half-lives are longer than $\sim$1 ns. The faster time response of the NRS measurement makes possible NRS experiments on nuclear levels with much shorter half-lives. We have fabricated an x-ray detector system that has a time resolution of 56 ps and a shorter tail function than that reported previously. With the implemented detector system, the NRS signal of the 26.27-keV state of ^{201}Hg could be clearly discriminated from the electronic scattering signal at an elapsed time of 1 ns after the SR pulse. The half-life of the state was determined as 629 $\pm$ 18 ps, which has better precision by a factor of three compared with that reported to date obtained from nuclear decay spectroscopy.

DOI: 10.1103/PhysRevC.97.024607

I. INTRODUCTION

Photonuclear excitation experiments using the high-brilliance x rays produced at synchrotron radiation (SR) facilities have been performed for various nuclei. Nuclear excitations are often conducted with these SR x rays for material science [1–4], where the nuclear motion correlated to phonon spectra within the material is probed by nuclear inelastic scatterings or nuclear forward scattering is used to obtain local electromagnetic information through the hyperfine interaction. These measurements are known as nuclear resonant scattering (NRS). The high-brilliance x rays from undulators and high-resolution monochromators can efficiently excite the relatively low-lying nuclear- levels below 100 keV [5,6]. The nuclear levels suited to these NRS experiments have been extended from 14.4 keV for ^{57}Fe as used in earlier experiments to the higher energies of 67.4 keV for ^{61}Ni [7] and 89.6 keV for ^{99}Ru [8] and the larger masses of 9.8 keV for ^{187}Os [9] and 26.3 keV for ^{201}Hg [10].

Likewise, half-life and radiative width of the excited state determined by NRS experiments are important as fundamental nuclear properties. Selective photonuclear excitations can extract the deexcitation signal with higher signal-to-noise ratio compared to radioactive decay or Coulomb excitation when there are no (or tiny) population to the relevant states in the decay spectroscopy measurements or the transition strengths to the excited state are small in the Coulomb excitation. It is also important that useless decay signals that tend to interfere with the true signal are absent in this selective excitation scheme.

Distinctive examples of such SR-based photonuclear excitation are the 29.83-keV level of ^{40}K [11] and the 26.27-keV level of ^{201}Hg [10]. The former cannot be populated by radioactive decay, and the accurate half-life and excitation energy obtained in NRS measurements are important for comparison with the results of nuclear reaction-induced spectroscopy, namely $(\alpha,n\gamma)$ [12] and (n,γ) [13]. The latter is weakly populated by electron-capture decay of ^{201}Tl, but the spectroscopic data have relatively large errors due to the small branching ratio to this level [14]. The half-life $T_{1/2}$ (26 keV) = 630(50) ps and the reduced transition matrix element of $B_{\mathrm{W.u.}}(M1) =$ 0.0263(23) in the database of Ref. [15] are taken from this decay experiment. Photonuclear excitation of the 26.27-keV level of ^{201}Hg was performed for materials sciences, and the level energy was measured precisely as 26.2738 $\pm$ 0.0003 keV [10]. However, the value of the half-life has not been updated in the photonuclear excitation due to its short half-life for NRS experiments. To date, the excited nuclear states used for NRS have been limited to levels whose half-lives are longer than

*yoshimi@okayama-u.ac.jp

$\sim$1 ns, with the half-life of the 26.27-keV level of ^{201}Hg being the shortest one.

Many heavier nuclei ($Z > 80$), including radioactive ones, have low-energy excited levels whose half-lives are shorter than 1 ns because the transitions from such levels tend to have large internal conversion coefficients. However, there are no SR-based NRS measurements for anything heavier than the Hg isotope. Some of them are levels whose half-lives have never been measured, such as the 9.2-keV, and 77.7-keV levels of ^{231}Pa and the 29.2-keV and 71.8-keV levels of ^{229}Th. In particular, ^{229}Th is known as an isotope with an extraordinarily low-lying isomer state of 7.8 ± 0.5 eV [16,17], 6.3–18.3 eV [18]. Because this isomer state is expected to be useful for precise nuclear clocks [19–21], the uncertainties in its nuclear properties should be investigated [22]. NRS experiments with such short-lived nuclear levels are important not only for material sciences but also for fundamental nuclear physics. Herein, we demonstrate such short-life NRS experimentally with the 26.27-keV level of ^{201}Hg by using a fabricated x-ray detector system that has fast time response and determines half-lives precisely. Furthermore, the photonuclear cross section and radiative decay width of the level are determined by evaluating the bandwidth of the monochromatized x-ray beam or comparison between the photonuclear excitation and photoelectric scattering counts.

II. NUCLEAR RESONANT SCATTERING OF 26.27-KEV STATE OF ^{201}Hg

The ^{201}Hg nucleus has a second excited state of 26.27 keV with $I^\pi = 5/2^-$. The transition between this level and the ground state with $I^\pi = 3/2^-$ is governed mainly by the $M1$ transition with a small $E2/M1$ mixing ratio of $\delta = 0.013(2)$ [14]. The photoexcitation cross section of the excited state at x-ray energies tuned to the resonance is

$$\sigma_{\mathrm{NRS}} = \frac{\lambda^2}{2\pi}\frac{2I_e+1}{2I_g+1}\frac{\Gamma_\gamma}{\Gamma_0}\frac{\Gamma_0}{\Gamma_{\mathrm{xray}}}, \tag{1}$$

which includes the effect of the x-ray bandwidth Γ_{xray}. Conventionally, this allows the NRS cross section to be compared directly to the photoelectric scattering cross section. Here λ is the wavelength of the incoming x rays, and I_g and I_e are the nuclear spins in the ground state and excited state, respectively. The term Γ_0 is the total decay width, which is related to the $(1/e)$ decay time from the excited state to the ground state. With the reported half-life, its value is estimated as $i\Gamma_0 = \hbar \ln 2/T_{1/2} \simeq 0.72$ μeV. The parameter Γ_γ is the radiative transition rate between the excited state and the ground state, which corresponds to its excitation width. Using the internal conversion coefficient α, the ratio between these two rates can be written as $\Gamma_\gamma/\Gamma_0 = 1/(1+\alpha)$. The internal conversion coefficient of the relevant ^{201}Hg transition is calculated as $\alpha = 71.6$ using the BrIcc code [23]. The excitation width is estimated as follows based on the reported half-life and the theoretical internal conversion coefficient:

$$\Gamma_\gamma = \frac{1}{1+\alpha}\frac{\hbar \ln 2}{T_{1/2}} \simeq 10\ \mathrm{neV}. \tag{2}$$

TABLE I. Parameters related to NRS experiments with ^{201}Hg. Internal conversion coefficients for subshell components are from Ref. [23]. Values of fluorescent yields are from Refs. [24,25]. Photoelectric absorption cross sections are from Ref. [26].

Nucleus	^{201}Hg
Excitation energy	26.272(25) keV
$I_g^\pi \rightarrow I_e^\pi$	$3/2^- \rightarrow 5/2^-$
Excitation width	10.0 neV
$T_{1/2}$ in excited state	0.630(50) ns
Internal conversion coefficient	$\alpha_{\mathrm{total}} = 71.6$ $\alpha_L = 55.5$ $\alpha_M = 13.0$
Fluorescence yield	$\omega_L = 0.35(1)$ $\omega_M \simeq 0.026$
Photoelectric absorption cross section at 26.27 keV	12.8 kb

The factor $\Gamma_0/\Gamma_{\mathrm{xray}}$ is introduced as the excitation efficiency of the incoming x rays, whose bandwidth Γ_{xray} is typically many orders of magnitude broader than the natural width Γ_0. The NRS cross section of the relevant ^{201}Hg excitation is thus $\sigma_{\mathrm{NRS}} = 18$ mb$(1b = 10^{-28}\ \mathrm{m}^2)$ when taking the typical singly monochromatized bandwidth of 10^{-4} ($\Gamma_{\mathrm{xray}} = 3$ eV) for SR. These parameters related to the nuclear resonance of ^{201}Hg are summarized in Table I.

Most incident x rays are absorbed photoelectrically by the orbital electrons of the target atoms. The contributions of Compton and Rayleigh scattering are negligibly small at x-ray energies around 26 keV. The cross section of photoelectric absorption for Hg atoms is $\sigma_{\mathrm{photoe}} = 12.8$ kb at a photon energy of 26.27 keV [26], which is larger than that of photonuclear excitation by six orders of magnitude. Using narrower-band x rays can reduce this large difference in cross section. The x-ray monochromatization with double Si monochromators is described in the following sections.

Sensitive detection of nuclear photoexcitation requires clear discrimination between the nuclear transition signal from the excited state and the fluorescence following the photoelectric process. The former signal occurs with a time delay due to the lifetime of the nuclear excited state. The latter signal occurs promptly on a subpicosecond time scale in the case of 26-keV radiation on a Hg target. The emitted photons in both processes have the same energy because the nuclear deexcitation is detected through the fluorescence following the internal conversion, as depicted in Fig. 1. The electrons from the Hg atoms are not detected in the experiment, as explained in the following section.

It is therefore important that the measurement system has a high temporal resolution to discriminate between these two processes. Furthermore, a slow tail component appearing in the detector time response in addition to a Gaussian function tends to affect such discrimination. Because the cross section of the prompt scattering is many orders of magnitude greater than that of the nuclear excitation, this tail component must be small, especially for measuring the short-lived nuclear levels. A detector whose time response has both a high temporal resolution and a short tail is essential. Conventional NRS

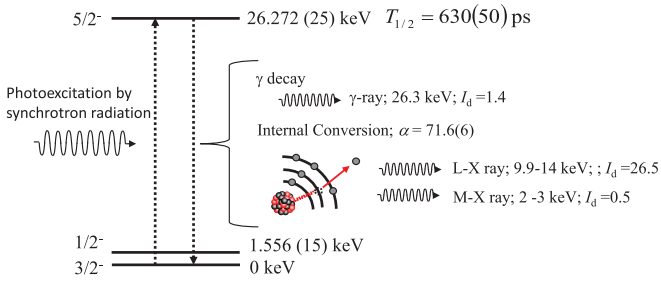

FIG. 1. Lower energy-level structure of ^{201}Hg and the decay scheme from the excited state. The relative decay intensity I_d is normalized for 10^2 decays from the excited state.

measurement uses counting gates after the SR excitation pulse [the full width at half maximum (FWHM) of which is typically 30–40 ps] to remove huge prompt background events. An Si avalanche photo diode (APD) of diameter 1–3 mm and depletion-layer depth of 10–30 μm is often used in NRS experiments; the typical time resolution of such an APD is 100–200 ps [27,28]. The counting gates start typically 2–5 ns after the synchrotron pulse in order to separate the NRS and prompt events [9–11]. A detector system for NRS measurement with higher time resolution is needed to measure the nuclear transitions precisely for short-lived excited-states. To demonstrate the feasibility of NRS experiments for short nuclear lifetimes, we show that it is possible to have clearly separated NRS and prompt events within a short elapsed time. We do this by collecting all the prompt and NRS scattering signals, without reducing their statistics, by using APD detectors that are faster than those used previously.

III. EXPERIMENT

The experiments were performed at the BL09XU beam line of SPring-8 [29]. The electron beam current in the storage ring was 100 mA, and the ring was operated in a 203-bunch mode with a 23.6-ns interval. The measured bunch width was 35 ps at FWHM. The x rays from the undulator were doubly monochromatized by Si(111) and Si(660) monochromators as shown in Fig. 2. The x rays reflected by the first Si(111) monochromator had a maximum intensity of 4×10^{13}

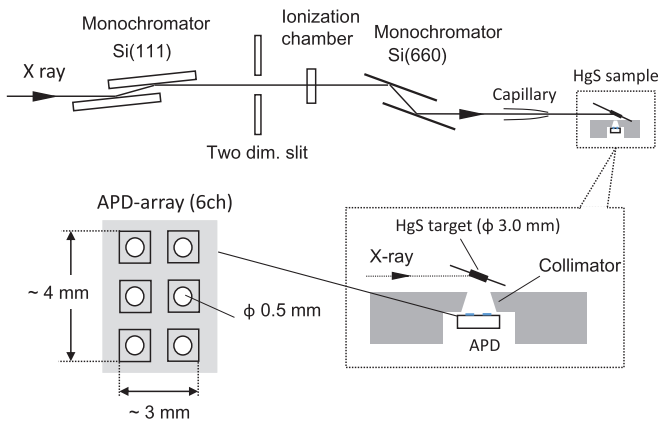

FIG. 2. Experimental setup for NRS of ^{201}Hg nucleus.

photons/s and a bandwidth of 3.4 eV (FWHM) at an energy of 26.27 keV. The angle of the Si(111) monochromator was set to obtain 26.27-keV x rays. The second Si(660) monochromator was used to reduce the bandwidth further. The incident x-ray beam was collimated to 0.8 mm × 0.8 mm by a two-dimensional slit and focused to a spot size of 0.3 mm × 0.2 mm at the target position by a tapered glass capillary (HORIBA, 2014SP13). The photon flux was monitored nondestructively using a small ion chamber, whose current was calibrated using a PIN photo diode (not shown in the figure). The photon fluxes measured at the target position with and without the capillary were 3.2×10^{11} photons/s and 3.7×10^{11} photons/s, respectively. An HgS powder with a 13.18% natural abundance of ^{201}Hg was used as the target material, which was located downstream of the beam line. A 4.8-mg quantity of HgS was pelletized to a disk of 3.0 mm diameter and 0.08 mm thickness. The number densities of $^{\rm nat}$Hg and ^{201}Hg were 2.1×10^{22} cm^{-3} and 2.8×10^{21} cm^{-3}, respectively. The HgS target was covered with two 100-μm-thickness beryllium plates. The electrons emitted from the target through photo-ionization and internal conversion were all stopped in the beryllium plate. The target was tilted at an angle of 25° to the beam direction.

Because of the large internal conversion coefficient, the NRS signal consisted mainly of characteristic L x rays following internal conversion of the excited nuclear state. These fluorescences were distributed in an energy range of 10–15 keV: $L_\alpha = 9.9$ keV, $L_\beta = 11.8$ keV, and $L_\gamma = 13.6$ keV. These signals coincide completely with the prompt signal in relation to energy because the incident 26.27-keV x rays induce photoelectric processes in the same electron shell. As summarized in Table I, the internal conversion of M-shell electrons also occurs with a coefficient of $\alpha_M = 13$. However, the fluorescence following M-shell conversion was not observable because of the small fluorescence yield of $\omega_M \simeq 0.026$. An Si-APD (S12053-05; Hamamatsu Photonics) with a small diameter of 0.5 mm and a thin depletion layer of 10 μm (as estimated from the data sheet) was used to detect the L-shell x-ray fluorescence. Such small and thin APD detectors tend to have relatively low detection efficiency but fast time response. Six Si-APD chips were mounted on a fabricated substrate to expand the sensitive area, as shown in Fig. 2. These were placed 3.5 mm away from the target sample. The solid angle of the APD-array system was $\Omega \simeq 80$ mstr. A cone-shaped brass collimator with diameters of 1.2 mm and 3.0 mm was placed between the target and the detector to reduce background x-ray scattering from different angles. Each APD output was amplified by a fast amplifier and was processed to a digital signal by a fast constant-fraction discriminator (CFD). Each event was labeled with its arrival time by a multistop time-to-digital converter (TDC; MCS6, FAST ComTec) with a resolution of 50 ps and was stored in a PC. This data acquisition was processed in parallel from the six APD chips to PCs. The analog pulse height of the APD signal was taken simultaneously in the TDC by using a fabricated analog-to-time converter (ATC). Two-dimensional analysis based on time and pulse height can reduce the background signal. This data-taking system can accept event rates up to ~1 MHz for each APD channel. Further details about the detector and data-acquisition system are given in Ref. [30].

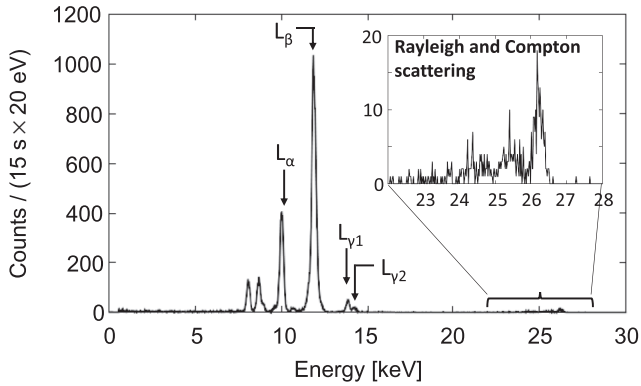

FIG. 3. Fluorescence energy spectrum from HgS target with 26.27-keV x-ray irradiation. The small peaks around 8 keV are characteristic x rays of Cu and Zn scattered from the brass around the target.

The rate of fluorescence detection associated with an NRS event is given by

$$R_{\mathrm{Hg\,NRS}} = N_{201\mathrm{Hg}}\sigma_{\mathrm{NRS}}\Phi_{\mathrm{xray}}\epsilon_{\mathrm{Lxray}}\epsilon_{\mathrm{eff}}, \quad (3)$$

where Φ_{xray} is the average photon flux density on the target, which was measured as $\Phi_{\mathrm{xray}} \simeq 1.4 \times 10^{12}$ photon/s/mm^2 within an area of 0.22 mm^2. The number of ^{201}Hg atoms irradiated by x rays was estimated to be $N_{201\mathrm{Hg}} \simeq (3.7 \times 10^{17}) \times 0.1318$ by considering an x-ray attenuation length of 0.038 mm in the Hg target. The emission probability $\epsilon_{\mathrm{Lxray}}$ of L-shell fluorescence is calculated to be $\epsilon_{\mathrm{Lxray}} = (\alpha_L/\alpha_{\mathrm{total}})\omega_L = 0.268$. The efficiency parameter ϵ_{eff} includes the APD detection efficiency, the solid-angle efficiency, the transmission ratio of fluorescence in the brass collimator, and fluorescence attenuation in the target. This parameter is uncertain because it depends on the alignment accuracy of the target, collimator, and detector. It is estimated roughly as $\epsilon_{\mathrm{eff}} = O(10^{-5})$. The NRS cross section $\sigma_{\mathrm{Hg\,NRS}}$ is estimated as 359 mb with Eq. (1) using the parameter values given in Table I. The linewidth Γ_{xray} of the incident x rays is determined to be 148 meV by measuring the energy spectrum of the NRS signal, as described in the following section.

The prompt-fluorescence detection rate is estimated by replacing $N_{201\mathrm{Hg}}$ and $\sigma_{\mathrm{Hg\text{-}NRS}}$ by $N_{\mathrm{Hg}} = (100/13.18)N_{201\mathrm{Hg}}$ and σ_{photoe}, respectively, in Eq. (3). The cross sections for the electron shells at this energy are obtained as $\sigma_L = 10.14$ kb and $\sigma_M = 2.48$ kb by interpolating from the data sheet of calculated values [31]. The L-x-ray emission probability is thus estimated as $\epsilon_{\mathrm{Lxray}} = (\sigma_L/\sigma_{\mathrm{photoe}})\omega_L = 0.279$. The L-shell fluorescence probability for NRS and prompt events is then almost the same within 0.27–0.28. Therefore, the relative NRS/prompt signal intensity is estimated extremely accurately, it being unaffected by the uncertainty in ϵ_{eff}. A typical energy spectrum of a prompt event is shown in Fig. 3. It was measured using an Si drift detector (SDD) at an incident x-ray energy of 26.27 keV to confirm the origin of the measured fluorescence. This indicates that the observed fluorescence consisted almost entirely of characteristic x rays of the L-shell. The measured amounts of Rayleigh and Compton scattering of the incoming x rays were estimated to be no more than 1% for all the measured fluorescence signals at the APD detector by considering the efficiency difference between two detectors: $\epsilon_{26\,\mathrm{keV}}/\epsilon_{12\,\mathrm{keV}} \simeq 0.17$ and 0.07 for the SSD and the APD, respectively.

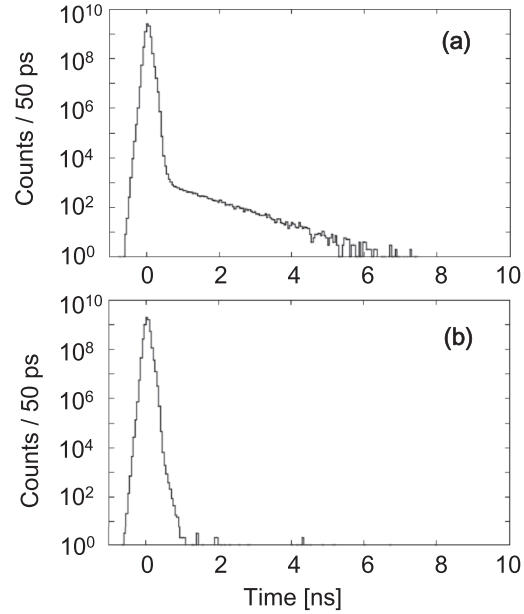

FIG. 4. (a) Typical time spectrum of fluorescence signal from HgS target with incident x-ray energy tuned to nuclear excitation of ^{201}Hg. (b) Time spectrum with incident x-ray energy detuned from resonance. Integration time was 2000 s for each spectrum.

IV. RESULTS AND DISCUSSION

A typical time spectrum measured when the incident energy was tuned to the $3/2^-(0\ \mathrm{keV}) \rightarrow 5/2^-$ (26.27 keV) transition of the ^{201}Hg nucleus is shown in Fig. 4(a). This spectrum contains both the prompt peak and the delayed NRS signal, the amplitude of the latter being six orders of magnitude smaller than the amplitude of the former. The only fluorescence events with their energies higher than 5 keV were collected in all spectra in this paper. The time resolution of the whole system was evaluated by χ-squared fitting a Gaussian function to the prompt peak. The standard-deviation width was found to be $\sigma = 56(2)$ ps. The intrinsic time resolution of the detector system was thus estimated to be $\sigma_{\mathrm{detector}} = 54$ ps by taking account of the SR pulse width of $\sigma_{\mathrm{SR}} = 15$ ps. The tail behavior of the prompt peak was evaluated from the time spectrum with the incident energy being far from resonance with the transition energy [Fig. 4(b)]. Here, the off-resonance time spectrum was taken with the incident energy detuned by 0.44 eV from the resonance center; it has a very short tail of less than 1 ns at 10^{-9}. This high time resolution and short tail compared to the previous measurements was realized by fabricating the detector and data-acquisition system specifically for the required timing resolution. This short tail of the detector time response enabled us to separate the pure NRS component from the prompt spectrum in a short elapsed time. The pure NRS spectrum was extracted in a time window of 0.9–5.2 ns and the half-life was then determined by χ-squared fitting a single exponential function to the NRS spectrum. We found that the reduced-χ^2

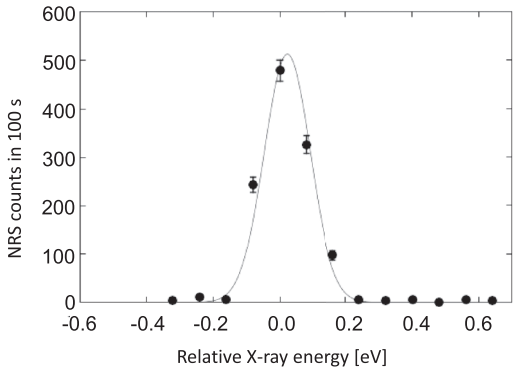

FIG. 5. NRS count as a function of incident x-ray energy controlled by scanning the Si monochromators. The width was found to be 148 ± 22 meV (FWHM).

ranged within 0.9–1.1 in the different fitting regions; the minimum range was 1.8–3.0 ns and the maximum range was 0.9–5.2 ns. The statistical and the systematic errors in the fitting procedure were obtained as 14 and 10 ps, respectively. A time jitter of 6 ps in the standard clock at SPring-8 [32], which was utilized in our data-acquisition system, produced an additional systematic effect. The half-life was then determined with a total uncertainty that is the quadratic sum of the statistical uncertainty and the systematic uncertainties, namely

$$T_{1/2}(26.27\ \text{keV}) = 629\ \pm 18\ \text{ps}. \tag{4}$$

This precision is better by a factor of three than the previous one that was determined from decay spectroscopy of ^{201}Tl [14], and the value is consistent within the error. The radiative transition width is calculated with the half-life and a theoretical internal conversion coefficient of $\alpha = 71.6(6)$ as $\Gamma_\gamma = 10.0(3)$ neV. The $M1$ reduced transition probability is thus determined precisely as

$$B_{\text{W.u.}}(M1) = \frac{\Gamma_\gamma/[\hbar(1+\delta^2)]}{3.15\times 10^{13}E_\gamma^3} = 0.0265 \pm 0.0008, \tag{5}$$

where the small $E2/M1$ mixing ratio $\delta = 0.013(2)$ is negligible in this calculation. The transition energy of $E_\gamma = 0.02627$ MeV is used in this calculation.

The resonance spectrum was obtained by plotting the delayed NRS counts in a time window of 1.0–5.0 ns along the incident x-ray energy, as shown in Fig. 5. The x-ray energy was scanned by controlling the angle of the Si(660) monochromator in steps of 0.26 s, which corresponds to an energy step of 83 meV. The width of this spectrum is dominated by the x-ray bandwidth (as determined by the double monochromator system) because this bandwidth is larger than the width of the nuclear level by many order of magnitude. The energy resolution of the monochromator system was determined as $\Gamma_{\text{xray}} = 148(22)$ meV (FWHM) by fitting a Gaussian function to each of the observed spectra and taking the average. From the determined bandwidth of the incident x rays and the above deduced radiative width Γ_γ, the effective NRS cross section [Eq. (1)] for ^{201}Hg is estimated as $\sigma_{\text{NRS}} = 0.36(5)$ b.

Measuring the whole time spectrum including both the prompt and delayed NRS components is effective for evaluating the consistency of the obtained data and then estimating the applicability to other nuclear targets. The ratio of the prompt count rate to the NRS one is expressed simply as $R_{\text{NRS}}/R_{\text{prompt}} = (N_{^{201}\text{Hg}}/N_{\text{Hg}}) \times (\sigma_{\text{NRS}}/\sigma_{\text{photoe}})$, as described previously. The obtained σ_{NRS} gives the ratio $R_{\text{NRS}}/R_{\text{prompt}} = 3.6\times 10^{-6}$, which is found to be consistent with the measured count rates of $R_{\text{NRS}} = 14$ Hz and $R_{\text{prompt}} = 3.6$ MHz in the spectrum shown in Fig. 4(a) to within the desired error. Both count rates are obtained consistently if the detector efficiency including the sensor area coverage and the fluorescence transmission through the collimator is $\epsilon_{\text{eff}} = 2.1\times 10^{-5}$ based on the measured x-ray flux density and estimated numbers of irradiated atoms, namely $N_{\text{Hg}} = 3.5\times 10^{17}$ and $N_{^{201}\text{Hg}} = 4.6\times 10^{16}$, respectively. The photon flux, which was monitored continuously in these measurements, was stable to within 1.5% (peak to peak) and was sufficiently reliable for the above estimation.

Conversely, the measured ratio $R_{\text{NRS}}/R_{\text{prompt}} = 3.9\times 10^{-6}$ (that is, $\sigma_{\text{NRS}} = 0.39$b) enabled us to determine the radiative width of the transition directly without the theoretical internal conversion coefficient as $\Gamma_\gamma = 10.8(16)$ neV using Eq. (1). This indicates that the internal conversion coefficient can be estimated from this radiative width and the measured total lifetime of this transition as $\alpha = 66(10)$. Although the error of this value is not small, it is consistent with the theoretical one within an acceptable error.

The present analysis shows that a radiative excitation width and a total decay width of an excited state can be determined independently. This enable us to determine γ-ray branching ratio from the excited state if the excited state have multiple branches to lower states. It can be conducted even if the energies of these different branches degenerate, a situation in which it is not possible to compare γ-ray intensities in decay spectroscopy experiments We should add that the present measurement system could be applied to nuclear levels with half-lives shorter than 0.6 ns. From the estimation with prompt width shown in Fig. 4(b), the NRS signal could be observed separately even when the half-life of the excited state is as short as $T_{1/2} \simeq 0.15$ ns and the NRS cross section is as small as $\sigma_{\text{NRS}} \simeq 30$ mb. The system could be improved further by increasing the number of APD-chips, or by focusing the incident x rays more with x-ray mirrors or lenses. The system could also be applied to radioactive nuclei that produce constant radiation backgrounds, where this background can be suppressed by appropriate selection of the energy window [30].

V. CONCLUSION

The 26.27-keV nuclear excitation of ^{201}Hg with high-brilliance synchrotron radiation and the measurement of its decay signal, known as nuclear resonant scattering, were investigated with a fabricated x-ray detector system tailored for fast time response. The measured time resolution of the entire system was 56 ps in standard deviation, and the time response had a short tail of 1 ns at 10^{-9}. Both NRS and prompt electronic scattering were observed with a high count rate of 3.6 MHz, and thus the half-life of the 26.27-keV excited state was determined as $T_{1/2}$ (26.27 keV) = 629 ± 18 ps, the

precision of which is better than the reported one obtained from nuclear decay spectroscopy by a factor three thanks to the high timing resolution. The radiative transition width and the photonuclear excitation cross section were also determined from this experiment. The present measurement system is an effective device for NRS experiments on nuclear levels with short half-lives (<1 ns).

ACKNOWLEDGMENTS

The synchrotron radiation experiments were performed at the BL09XU of SPring-8 with the approval of the Japan Synchrotron Radiation Research Institute (JASRI) (Proposals No. 2014A1334, No. 2014B1254, No. 2015B1380, No. 2016A1420, and No. 2016B1232). This works was partially performed under the joint research project at International Research Center for Nuclear Materials Science, Institute for Materials Research, Tohoku University. This work was also supported by JSPS KAKENHI Grants No. 15H03661, No. 17K14291, and No. 24221005; Technology Pioneering Projects in RIKEN; and MATSUO FOUNDATION. S.S. and T.S. received funding from the European Union's Horizon 2020 research and innovation programme under Grant Agreement No. 664732.

[1] E. Gerdau, R. Ruffer, H. Winkler, W. Tolksdorf, C. P. Klages, and J. P. Hannon, Phys. Rev. Lett. **54**, 835 (1985).
[2] J. B. Hastings, D. P. Siddons, U. van Burck, R. Hollatz, and U. Bergmann, Phys. Rev. Lett. **66**, 770 (1991).
[3] M. Seto, Y. Yoda, S. Kikuta, X. W. Zhang, and M. Ando, Phys. Rev. Lett. **74**, 3828 (1995).
[4] R. Röhlsberger, *Nuclear Condensed Matter Physics with Synchrotron Radiation* (Springer, Berlin, 2004).
[5] M. Seto, J. Phys. Soc. Jpn. **82**, 021016 (2016).
[6] Y. Yoda, M. Yabashi, K. Izumi, X. W. Zhang, S. Kishimoto, S. Kitao, M. Seto, T. Mitsui, T. Harami, Y. Imai, and S. Kikuta, Nucl. Instrum. Methods A **467-468**, 715 (2001).
[7] I. Sergueev, A. I. Chumakov, T. H. Deschaux Beaume-Dang, R. Rüffer, C. Strohm, and U. van Bürek, Phys. Rev. Lett. **99**, 097601 (2007).
[8] D. Bessas, D. G. Merkel, A. I. Chumakov, R. Rüffer, R. P. Hermann, I. Sergueev, A. Mahmoud, B. Klobes, M. A. McGuire, M. T. Sougrati, and L. Stievano, Phys. Rev. Lett. **113**, 147601 (2014).
[9] D. Bessas, I. Sergueev, D. G. Merkel, A. I. Chumakov, R. Rüffer, A. Jafari, S. Kishimoto, J. A. Wolny, V. Schünemann, R. J. Needham, P. J. Sadler, and R. P. Hermann, Phys. Rev. B **91**, 224102 (2015).
[10] D. Ishikawa, A. Q. R. Baron, and T. Ishikawa, Phys. Rev. B **72**, 140301(R) (2005).
[11] M. Seto, S. Kitao, Y. Kobayashi, R. Haruki, T. Mitsui, Y. Yoda, X. W. Zhang, and Yu. Maeda, Phys. Rev. Lett. **84**, 566 (2000).
[12] F. Brandolini, C. Rossi Alvarez, G. B. Vingiani, and M. de Poli, Phys. Lett. B **49**, 261 (1974).
[13] J. F. Boulter, W. V. Prestwich, and B. Arad, Can. J. Phys. **47**, 591 (1969).
[14] P. Schüler, K. Hardt, C. Günther, K. Freitag, P. Herzog, H. Niederwestberg, and H. Reif, Z. Phys. A **313**, 305 (1983).
[15] F. G. Kondev, Nucl. Data Sheets **108**, 365 (2007).
[16] B. R. Beck, J. A. Becker, P. Beiersdorfer, G. V. Brown, K. J. Moody, J. B. Wilhelmy, F. S. Porter, C. A. Kilbourne, and R. L. Kelley, Phys. Rev. Lett. **98**, 142501 (2007).
[17] B. R. Beck, C. Y. Wu, P. Beiersdorfer, G. V. Brown, J. A. Becker, J. K. Moody, J. B. Wilhelmy, F. S. Porter, C. A. Kilbourne, and R. L. Kelley, Lawrence Livermore National Laboratory, Conference LLNL-PROC-415170, 2009, http://www.osti.gov/scitech/biblio/964521-r2Qnkb/.
[18] L. von der Wense, B. Seiferle, M. Laatiaoui, J. B. Neumayr, Hans-Jorg Maier, Hans-Friedrich Wirth, C. Mokry, J. Runke, K. Eberhardt, C. E. Dullmann, N. G. Trautmann, and P. G. Thirolf, Nature **533**, 47 (2016).
[19] E. Peik and Chr. Tamm, Europhys. Lett. **61**, 181 (2003).
[20] G. A. Kazakov, A. N. Litvinov, V. I. Romanenko, L. P. Yatsenko, A. V. Romanenko, M. Schreitl, G. Winkler, and T. Schumm, New J. Phys. **14**, 083019 (2012).
[21] C. J. Campbell, A. G. Radnaev, A. Kuzmich, V. A. Dzuba, V. V. Flambaum, and A. Derevianko, Phys. Rev. Lett. **108**, 120802 (2012).
[22] E. V. Tkalya, C. Schneider, J. Jeet, and E. R. Hudson, Phys. Rev. C **92**, 054324 (2015).
[23] Internal conversion coefficient data base BrIcc, http://bricc.anu.edu.au/.
[24] J. H. Hubbell, P. N. Trehan, N. Singh, B. Chand, D. Mehta, M. L. Garg, R. R. Garg, S. Singh, and S. Purl, J. Phys. Chem. Ref. Data **23**, 339 (1994).
[25] W. Bambynek, B. Crasemann, R. W. Fink, H.-U. Freund, H. Mark, C. D. Swift, R. E. Price, and P. V. Rao, Rev. Mod. Phys. **44**, 716 (1972).
[26] NIST Photon cross-section databases, https://www.nist.gov/pml/xcom-photon-cross-sections-database.
[27] S. Kishimoto, Nucl. Instrum. Methods A **351**, 554 (1994).
[28] A. Q. R. Baron, S. Kishimoto, J. Morsec, and J.-M. Rigal, J. Synchrotron Radiat. **13**, 131 (2006).
[29] Y. Yoda, Y. Imai, H. Kobayashi, S. Goto, K. Takeshita, and M. Seto, Hyperfine Interact. **206**, 83 (2012).
[30] T. Masuda, S. Okubo, H. Hara, T. Hiraki, S. Kitao, Y. Miyamoto, K. Okai, R. Ozaki, N. Sasao, M. Seto, S. Uetake, A. Yamaguchi, Y. Yoda, A. Yoshimi, and K. Yoshimura, Rev. Sci. Inst. **88**, 063105 (2017).
[31] J. H. Scofield, Lawrence Livermore National Laboratory Rep. UCRL-51326 (1973).
[32] H. Suzuki, H. Ego, M. Hara, T. Hori, Y. Kawashima, Y. Ohashi, T. Ohshima, N. Tani, and H. Yonehara, Nucl. Instrum. Methods Phys. Res. A **431**, 294 (1999).